



In situ co-precipitation preparation of a superparamagnetic graphene oxide/Fe₃O₄ nanocomposite as an adsorbent for wastewater purification: synthesis, characterization, kinetics, and isotherm studies

Shengyan Pu¹ · Shengyang Xue¹ · Zeng Yang¹ · Yaqi Hou¹ · Rongxin Zhu¹ · Wei Chu²

Received: 11 December 2017 / Accepted: 26 March 2018 / Published online: 13 April 2018

© Springer-Verlag GmbH Germany, part of Springer Nature 2018

Abstract

A superparamagnetic graphene oxide (GO)/Fe₃O₄ nanocomposite (MGO) was prepared by a facile in situ co-precipitation strategy, resulting in a prospective material for the application of graphene oxide in wastewater treatment. MGO was characterized by scanning electron microscopy (SEM), transmission electron microscopy (TEM), x-ray diffraction (XRD), and Fourier transform infrared spectroscopy (FTIR). The prepared adsorbent showed a high adsorption efficiency relevant to the purification of dye-contaminated wastewater and could be readily magnetically separated. The maximum adsorption capacity was ca. 546.45 mg g⁻¹ for the common cationic dye methylene blue (MB) and ca. 628.93 mg g⁻¹ for the anionic dye Congo red (CR). The adsorption processes fit the pseudo-second-order kinetic model well, which revealed that these processes may involve the chemical interaction between adsorbate and adsorbent. The thermodynamic parameters indicated that the adsorption reaction was an endothermic and spontaneous process. Furthermore, the prepared magnetic adsorbent had a wide effective pH range from 5 to 11 and showed good stability after five reuse cycles. The synthetic MGO showed great potential as a promising adsorbent for organic contaminant removal in wastewater treatment.

Keywords In situ co-precipitation · Graphene oxide · Magnetic adsorbent · Dyeing wastewater

Introduction

Pollution from dye wastewater has drawn worldwide public concern due to its high biological toxicity, carcinogenicity, teratogenicity, and mutagenicity in living organisms, especially human beings (Belpaire et al. 2015, Forgacs et al. 2004). Various methods such as chemical oxidation (Lucas and Peres

2006, Pu et al. 2017a), photochemical catalysis (Pu et al. 2017b), membrane separation (Ma et al. 2017, Netpradit et al. 2003), electrochemical degradation (Riera-Torres et al. 2011, Szpyrkowicz et al. 2001), and biodegradation (Malachova et al. 2013), have been developed for the purification of dye wastewater. However, the application of these techniques has been limited due to their inevitable drawbacks, such as high energy consumption, secondary pollution, and high operating costs. Beyond the techniques listed above, adsorption is considered to be one of the strategies with the most potential due to its advantages of easy operation, low energy consumption, few harmful byproducts, the possibility of adsorbent recycling, etc. (Ma et al. 2018). Adsorption approaches may be based on various adsorbents such as chitosan (Pu et al. 2017d), activated carbon (Greenwald et al. 2015), clay (Abidi et al. 2015), and bio-waste (Kyzas et al. 2013). Unfortunately, the practical application of adsorbents has been limited by their poor utilization rate, difficult recovery, and low adsorption capacity (Akbari et al. 2002).

Graphene oxide (GO) and graphene-based composite materials are attracting tremendous research interest as a novel adsorbent for environmental purification due to their

Shengyan Pu and Shengyang Xue contributed equally to this work.

Responsible editor: Guilherme L. Dotto

Electronic supplementary material The online version of this article (<https://doi.org/10.1007/s11356-018-1872-y>) contains supplementary material, which is available to authorized users.

✉ Shengyan Pu
pushengyan@gmail.com; pushengyan13@cdut.cn

¹ State Key Laboratory of Geohazard Prevention and Geoenvironment Protection, Chengdu University of Technology, 1#, Dongsanlu, Erxianqiao, Chengdu 610059, Sichuan, People's Republic of China

² Department of Civil and Environment Engineering, The Hong Kong Polytechnic University, Hong Kong, People's Republic of China

enormous specific surface area (1000–1217 m² g⁻¹) (Tang et al. 2010), large number of active sites (Dreyer et al. 2010), and excellent dispersibility (Cheng et al. 2017). Its hydrophilic oxygen-containing functional groups (e.g., carboxyl, hydroxyl, and epoxy functional groups) (Dreyer et al. 2010, Huang et al. 2016) allow GO to combine easily with hydrophilic and hydrophobic compounds (e.g., heavy metals, dyes, and sediment), which gives GO great potential in wastewater treatment (Liu et al. 2012). GO has been proven to possess great potential as superior adsorbent for removing many kinds of organic and inorganic contaminants including heavy metal ions (Peng et al. 2017b), uranium (VI) (Zhang et al. 2016b), fluoride (Barathi et al. 2014), methylene blue (Zhang et al. 2016a), dibenzothiophene (Dizaji et al. 2016), and polyphenols (Peng et al. 2017a). Recently, magnetic graphene oxide has been widely used as a new magnetic solid-phase extraction adsorbent in environmental purification applications (Aliyari et al. 2016). In general, magnetic adsorbents are often composed of magnetic nanoparticles dispersed in a cross-linked polymer matrix, including natural and synthetic polymers (Yao et al. 2012). However, these methods suffer many drawbacks such as high cost, complicated operation, and easy clogging.

In this study, we primarily focused on developing a recyclable, multi-functional, and high-efficiency adsorbent for dye wastewater purification. We prepared a superparamagnetic graphene oxide/Fe₃O₄ hybrid nanocomposite (MGO) via an in situ co-precipitation strategy, which was successfully obtained through a facile and green in situ synthetic approach. The common dyes Congo red (CR, anionic dye) and methylene blue (MB, cationic dye) were used to evaluate its adsorption properties. Batch experiments under varied influential parameters, such as initial pH, dye concentration, temperature, and coexisting ions, were conducted to assess the properties of MGO. The synthesized MGO demonstrated good performance for dye removal and a wide range of abilities to adsorb many types of dyes, including both anionic and cationic dyes. The results demonstrate potential for the application of graphene oxide in wastewater treatment.

Materials and methods

Materials

The graphite powder was purchased from Aladdin Reagent Factory (Shanghai, China). Sodium nitrate (NaNO₃, ≥ 99.9%); sulfuric acid (H₂SO₄, 98%); potassium permanganate (KMnO₄, 65–68%); hydrogen peroxide (H₂O₂, 30 wt%); ammonia (NH₄OH, 25–28%); ethanol (C₂H₅OH, ≥ 99.9%); MB; and CR were provided by Chengdu Kelong Chemical Reagent Company (Sichuan, China). FeCl₂·4H₂O and FeCl₃·6H₂O were purchased from Tianjin Zhiyuan Chemical Reagent

Company (Tianjin, China). All chemical reagents were analytical grade and used without further purification. Deionized water used for all experiments was generated from Milli-Q water purification system (Ulupure Corporation, CA).

Experimental section

Preparation of graphene oxide

Graphene oxide was synthesized from graphite powder via a modified Hummers method (Stankovich et al. 2006). Typically, 2.0 g graphite powder and 1.2 g sodium nitrate were added into 60 mL concentrated sulfuric acid (98%) solution in a three-neck flask immersed in an ice bath while maintaining mechanical stirring. A total of 8.8 g potassium permanganate was slowly added into the flask and the temperature was cooled to 278.15 K for 12 h. Subsequently, 72 mL distilled water was added dropwise into the mixture at 293.15 K, and the mixture was stirred at 323.15 K overnight. After the color of the mixture turned bright yellow, 22 mL H₂O₂ solution was added gradually into the mixture for 2 h. The mixture was washed successively with 5% HCl solution and deionized water until the pH of the rinse water became neutral, after which it was freeze-dried (Scientz-50F, China) for more than 32 h. Finally, 0.3 g GO was dispersed in 100 mL water by an ultrasonic cell disruptor to obtain a GO dispersion (3 mg mL⁻¹).

Preparation of magnetic graphene oxide nanocomposite

The magnetic graphene oxide nanocomposite (MGO) was synthesized by a chemical in situ co-precipitation method. Briefly, 1.3 mmol FeCl₂·4H₂O and 2.6 mmol FeCl₃·6H₂O were dissolved in 400 mL deionized water under an N₂ atmosphere. An appropriate molar ratio of FeCl₂ and FeCl₃ was adopted (1:2) to meet the stoichiometric requirement. To prevent the aggregation of the GO sheets in a low pH (pH = 1.89) environment, 0.7 mL NH₃·H₂O was used to adjust the pH before adding 100 mL GO. Then, 40 mL NH₃·H₂O was continuously added with vigorous stirring for 3 h at 353.15 K. Finally, the black precipitate was washed several times with deionized water and ethanol to remove the residual alkali solution, which was heated at 333.15 K in vacuum conditions for 8 h.

Batch adsorption experiments

Two typical cationic and anionic dyes, MB and CR, were used as representative contaminants to evaluate the adsorption properties of MGO. All batch adsorption experiments were performed in a constant temperature shaker. Briefly, adsorption experiments were carried out by adding 25 mg MGO powder into 50-mL dye solution in a shaker (298.15 ±

0.5 K) for 24 h to reach adsorption equilibrium. The adsorbent was removed by magnetism and the remaining concentration of dye was measured by a visible spectrophotometer (V-1100D, Mita, Shanghai) at wavelengths of 664 nm for MB and 497 nm for CR. The adsorption capacity (q_e) of MGO was calculated using Eq. (1) (Ren et al. 2013) as the following:

$$q_e = \frac{(C_0 - C_t)V}{m} \quad (1)$$

The removal rates (η) of the dyes were determined by using Eq. (2):

$$\eta = \frac{C_0 - C_t}{C_0} \quad (2)$$

where C_0 (mg L⁻¹) is the initial concentration of the test solution, C_t is the concentration of the test solution (mg L⁻¹) at time t (min), V (L) is the volume of the test solution, and m (g) is the weight of the adsorbent. All experiments were performed in three parallel groups for accuracy.

To assess the effects of initial pH, different temperatures, and initial concentration of dye on adsorption, consistent conditions were maintained except when changing the experimental variable. To investigate the effect of initial pH on adsorption, pH was adjusted by adding a small amount of HCl (1 mol L⁻¹) and NaOH (1 mol L⁻¹) while the solution volume and other conditions were constant. To assess the effects of different temperature, the reaction temperatures were adjusted by the water bath from 298.15 to 328.15 K \pm 0.5 K. The effect of the initial dye concentration was measured by adsorbing different concentrations of dye (from 50 to 1500 mg L⁻¹). The effect of coexisting ions on adsorption was studied by adding known amounts of Na⁺, Ca²⁺, K⁺, NO₃⁻, Cl⁻, and HPO₄⁻. The concentration of the residual dye was analyzed at established time intervals during the adsorption process.

Desorption studies

To evaluate the stability and reusability of the adsorbent, the adsorbent was collected from solution after reaching equilibrium and washed several times with ethanol, NaOH (1 mol L⁻¹) and deionized water before being reused for the next adsorption. The above process was repeated five times.

Characterization

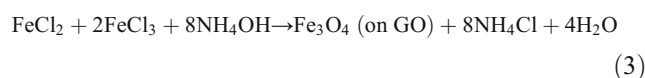
The crystal structure of MGO was characterized by XRD (Ultima IV, Japan) employing CuK α radiation (λ = 0.154 nm, 40 kV) in the range of 3° to 80°. FTIR (Nicolet-1170 SX, USA) was used to analyze the functional groups of MGO with the KBr wafer technique. The scanning wavelength range was from 400 to 4000 cm⁻¹. The surface

morphology was characterized by SEM (SIGMA300, Germany) at a voltage of 20 kV. The micromorphology was observed by TEM (JEM2100, Japan) operated at 200 kV. The magnetic properties were recorded at room temperature with a vibrating sample magnetometer (VSM) (730 T Lakeshoper, America). Samples were pretreated by heating under vacuum at 403.15 K for 10 h.

Results and discussion

Preparation and characterization of MGO

The MGO composite was synthesized through a chemical in situ co-precipitation approach (Fig. 1a). The color of the mixture rapidly changed from dark brown to black after NH₃·H₂O addition (Fig. 1b), as the in situ co-precipitation reaction between the Fe³⁺, Fe²⁺ mixture, and alkali solution formed magnetic Fe₃O₄ nanoparticles with the following reaction (Yang et al. 2012):

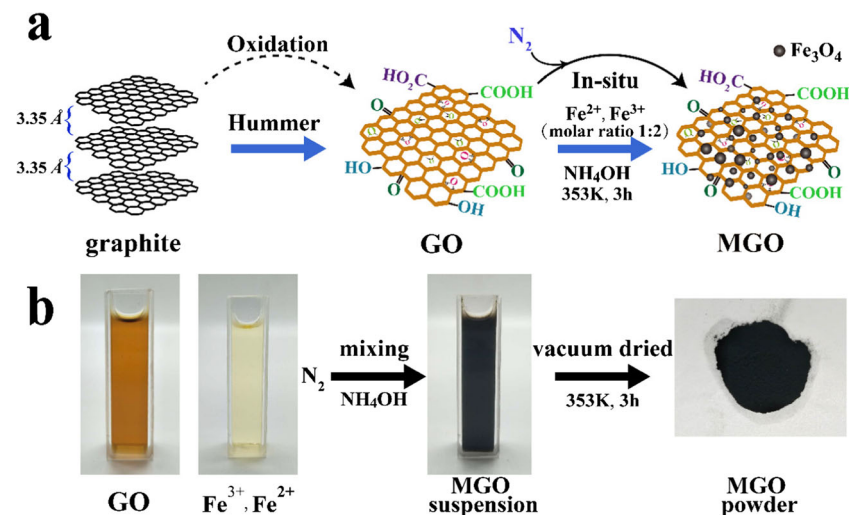


The color of mixture turned from brown to black, indicating the formation of Fe₃O₄. The resulting MGO powder was a black sand-like powder (Fig. 1b).

The crystalline phases of the pure Fe₃O₄, GO, and synthesized MGO were identified with XRD (Fig. 2a). The characteristic diffraction peaks at 2θ = 30.10°, 35.4°, 43.11°, 56.28°, and 62.74°, corresponded with the planes at (220), (311), (400), (511), and (440), respectively, which is in strong accordance with Fe₃O₄ nanoparticles (JCPDS No. 19-0629) (Wang et al. 2015). The GO displayed a broad diffraction peak ranging from 15° to 30°. The XRD pattern of MGO exhibited similar XRD patterns to Fe₃O₄ and the characteristic diffraction peaks matched well with those of Fe₃O₄. There was a weak diffraction peak of GO detected in the MGO, possibly due to the strong diffraction peaks of Fe₃O₄, which made the GO peak (25°) appear weak, indicating that the crystalline structure of GO was not changed substantially during synthesis. The EDX element distribution of MGO is shown in Fig. S1. The peaks of O, C, and Fe indicated that Fe compounds were successfully introduced into the GO surface. Based on XRD analysis, we can describe the composite formed by Fe₃O₄ and GO.

The FTIR spectra of GO, Fe₃O₄, and MGO are shown in Fig. 2b. The pure GO curve showed obvious characteristic absorption peaks at 3397, 1737, 1627, 1399, and 1079 cm⁻¹. The adsorption bands at 3397 and 1627 cm⁻¹ were attributed to -OH stretching and C=C stretching vibrations. The bands at 1737 and 1399 cm⁻¹ were mainly

Fig. 1 a) Schematic illustration of MGO preparation via in situ co-precipitation. The graphene oxide was prepared by a modified Hummer's method. b) Photographs of GO solution, combined Fe³⁺ and Fe²⁺ solution, MGO suspension, and the obtained MGO powder

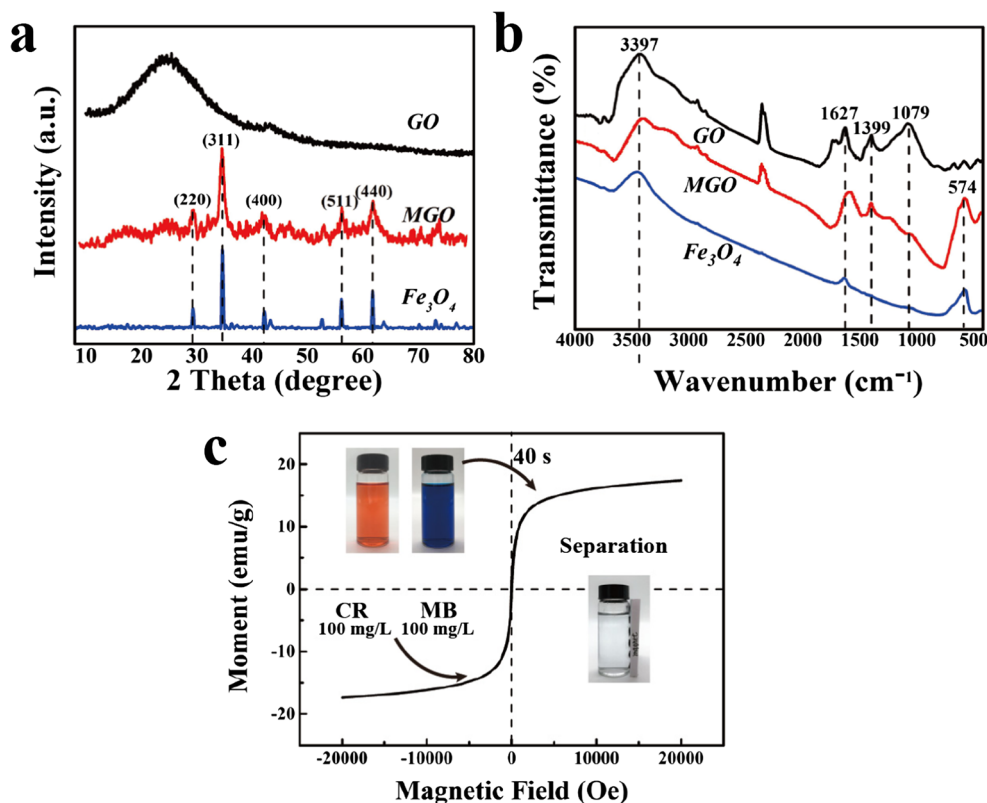


ascribed to C=O and O–C=O stretching vibrations. The band at 1079 cm⁻¹ was attributed to the stretching vibration of sp² hybridized of C–O–C. A comparison of GO to MGO showed that the characteristic peaks at 1737 and 1079 cm⁻¹ disappeared, and a peak at 574 cm⁻¹ emerged which was assigned to the Fe–O stretching vibration. Data analyses indicated that the Fe₃O₄ nanoparticles were successfully embedded in the graphene oxide. Therefore, it was evident that some functional groups of GO were reduced via the in situ co-precipitation process (Wan and

Wang 2017). Moreover, the dye adsorption by MGO could be attributed to hydrogen bonding interactions between O–C=O, –OH, and the dye's characteristic groups. Carboxyl O–C=O groups were responsible for interactions between the D–SO₃⁻ (D = dye molecule) and the MGO.

The magnetic performance of the prepared MGO nanocomposite was determined by VSM. Typical magnetization hysteresis loops were recorded and are illustrated in Fig. 2c. The saturation magnetization was found to be 17.38 emu g⁻¹. The magnetization curve of MGO was close to an “S” curve

Fig. 2 a) XRD patterns of GO, MGO, and Fe₃O₄. b) FTIR spectra of GO, MGO, and pure Fe₃O₄ NPs. c) Magnetic hysteresis loops of MGO. Conditions: initial MB/CR concentration 100 mg L⁻¹, adsorbent dosage 0.5 g L⁻¹, temperature 298 ± 0.5 K, stirring rate 180 rpm



and the coercivity was negligible (nearly zero), indicating that no magnetization remained after removing the external magnetic field (Ren et al. 2013). Therefore, the superparamagnetic behavior of nanocomposite MGO was established. Moreover, the inset in Fig. 2c illustrates the color change in the dye solution before and after adsorption. The adsorbent dosage was 0.5 g L^{-1} and the initial dye concentration was 100 mg L^{-1} . After adsorption reaction, the MGO was easily separated from aqueous solution within 40 s under a magnetic field, and the supernatant was colorless, as shown in Fig. 2c. Thus, the obtained MGO had highly efficient adsorption (removal rate can reach 99%) properties and could be readily magnetically separated.

Subsequently, the morphology of GO and MGO was studied by SEM and TEM. SEM images of GO (Fig. 3a) revealed that the GO had a smooth surface with many wrinkles, which led to its large specific surface area and abundant active sites. The prepared GO presented a typical multi-layered structure and the surface was relatively rough (Fig. 3b). Transmission electron microscopy (TEM) was performed to elucidate the morphology and structure of the MGO compound. It was clear that the elliptical and circular Fe_3O_4 nanoparticles were uniformly dispersed on the translucent graphene oxide substrate with an average diameter of ca. $\sim 9.8 \text{ nm}$ (Fig. 3d, inset), which indicated that the Fe_3O_4 nanoparticles were successfully loaded on the GO sheets.

Adsorption experiments

The initial pH was one of the most important factors in the adsorption process, influencing not only the surface charge of the adsorbent but also the functional groups on the GO and the chemical properties of the dye solution. The anionic dye CR

and cationic dye MB were used to investigate the pH sensitivity of MGO, and the experimental pH values varied from 3 to 11. The results indicated that the adsorption of MGO on MB was insensitive to pH value changes. The equilibrium adsorption capacity of MB was higher than 180.2 mg g^{-1} , and increased smoothly upon increasing the solution pH (Fig. 4a). There are two acid–base equilibriums of MB and GO, represented by $\text{GO-H} \rightarrow \text{GO}^- + \text{H}^+$ and $\text{MBH}^{2+} \rightarrow \text{MB}^+ + \text{H}^+$ (Zhang et al. 2011). The amount of hydrogen ions increased with decreasing pH values, thus competing more with the MB cations. Due to the abundance of H^+ , GO-H was the main form of GO^- which decreased the amount of MB adsorbed. In contrast, there was more GO^- at higher pH values, which may have enhanced the electrostatic attraction between MGO and MB, thus increasing the adsorption capacity for MB. However, it can be clearly seen from Fig. 4b that the adsorption curve of CR showed a different pattern from that of MB. The equilibrium adsorption capacity decreased sharply at low pH values (pH = 3), dropping from 189.4 to 34.1 mg g^{-1} . The reason for this phenomenon might be because CR is a reactive indicator dye, and its structure changed with the change in pH value. At a low initial pH range (pH < 3.5), the $-\text{NH}_2$ of CR would protonate to $-\text{NH}_3^+$ (Fig. S2), which decreased the electrostatic repulsive force between CR and MGO. The decrease of electrostatic repulsion in acidic condition was favorable to physical adsorption. However, according to the adsorption kinetics, it was found that the adsorption were mainly chemical adsorption, and these protonated functional groups would not be conducive to chemical adsorption. When the pH was lower than the acid dissociation constant of oxygen-containing groups, these groups became positively charged (C-OH_2^+ , C-COOH_2^+), as a result of which the main interactions between CR and MGO were

Fig. 3 SEM images of **a**) GO and **b**) MGO. TEM images of **c**) GO and **d**) MGO and size distribution of Fe_3O_4 nanoparticles formed inside the MGO

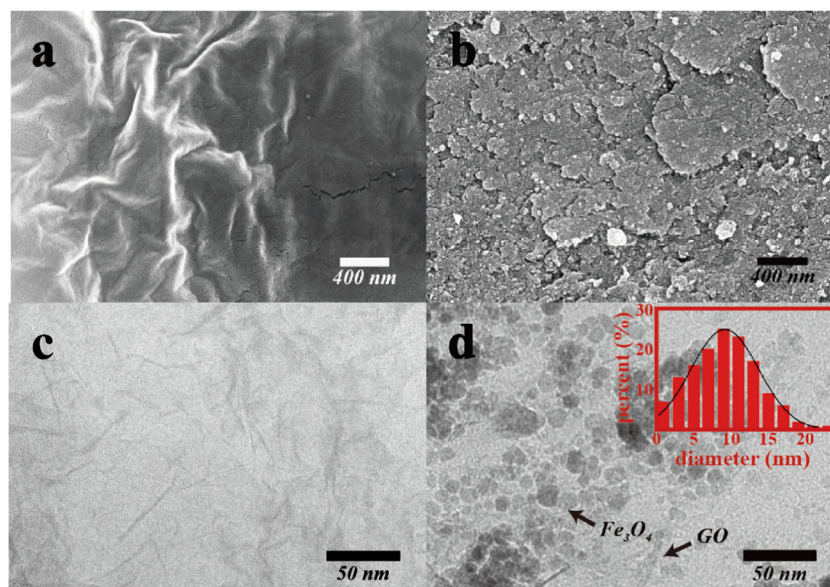
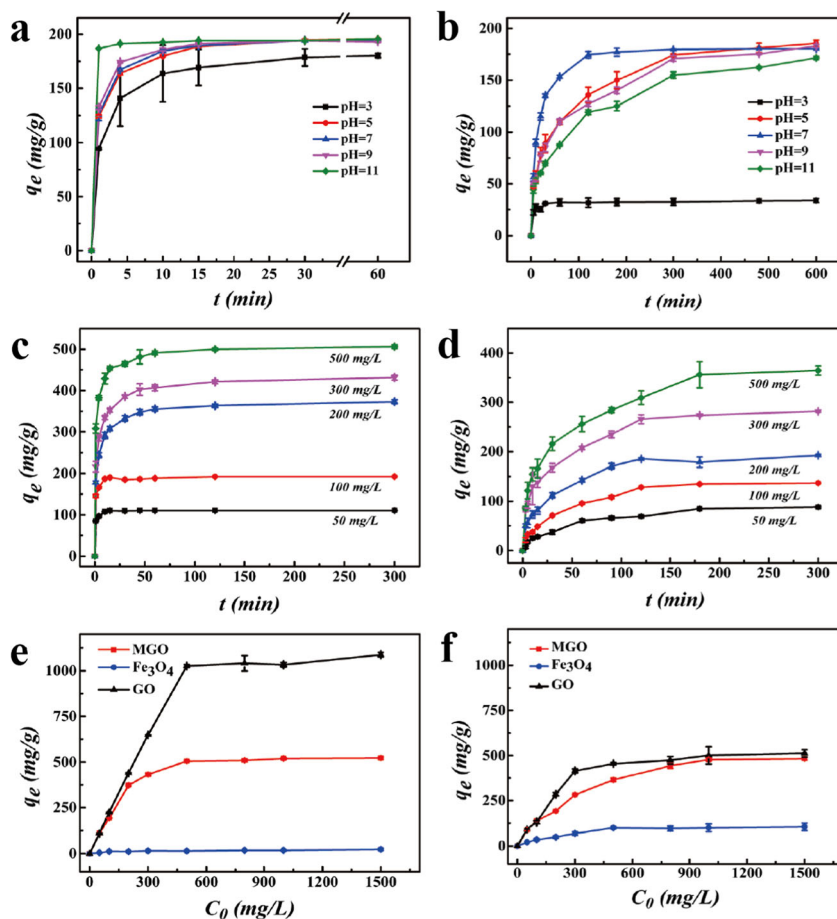


Fig. 4 Effect of initial pH on MB (a) and CR (b) adsorption. Conditions: initial MB/CR concentration 100 mg L⁻¹, adsorbent dosage 0.5 g L⁻¹, temperature 298 ± 0.5 K, and stirring rate 180 rpm. Effects of adsorption times and initial dye concentrations of MB (c) and CR (d) on MGO adsorption capacity. Effect of initial MB (e) and CR (f) dye concentration on adsorption of MGO, Fe₃O₄, and GO.



chemical bonds (Ahmad and Kumar 2010). The active sites at the surface of the adsorbent may determine the adsorption capacity of MGO.

With increasing pH, the zeta potential of MGO becomes negative. The zeta potential value decreased steadily from 12 to -50 mV (Fig. S3) as the pH increased from 2 to 11. It was observed that the adsorption capacity of MB increased with decreasing zeta potential value, due to the increase of the Coulombic force between MB molecules and MGO.

The effect of initial concentration was systematically investigated. Figure 4c, d compare the adsorption performance at various initial concentrations (i.e., 50, 100, 200, 300, 500 and 800 mg L⁻¹ of MB and CR). The results showed that the dye adsorption capacity gradually increased as the initial concentration increased. The adsorption capacity of MGO increased rapidly during the first 5 min, and the initial concentration of the solution had little effect on the adsorption rate (Fig. 4c, d). As the concentration of the dye solution increased, there was a significant increase in adsorption capacity. After a long period of time, the adsorption capacity increased slowly and eventually reached equilibrium. The surface sites may have been occupied by dye molecules, causing a decrease in adsorption rate.

Furthermore, Fig. 4e, f compare the different adsorption properties of MGO, Fe₃O₄, and GO for dye removal. The theoretical maximum equilibrium adsorption capacity of MGO, GO, and Fe₃O₄ were 1.4615, 2.8974, and 0.0591 mmol g⁻¹ for MB and 0.9028, 0.7476, and 0.1721 mmol g⁻¹ for CR (Table S3), respectively. The adsorption capacity of CR (36.2674 mg g⁻¹) on Fe₃O₄ was better than that of MB (12.8027 mg g⁻¹) because the Fe₃O₄ was positively charged in aqueous solution and therefore favored CR adsorption. The theoretical maximum adsorption capacities of MB (193.0502 mg g⁻¹) and CR (150.3759 mg g⁻¹) on MGO have similar values. However, upon comparing the dyes' K_L values and rates of adsorption (r), the MB adsorption rate ($K_L = 0.0885$, $r = 0.75$) was much faster than that of CR ($K_L = 0.0178$, $r = 0.02$) (Table S3). The adsorption of MB (225.225 mg g⁻¹) on GO was significantly higher than that of CR (138.1215 mg g⁻¹), which may be due to difference in the dyes' structures and characteristics.

The BET surface areas of GO and MGO were measured as 1115.3468 and 407.1267 m² g⁻¹, respectively, suggesting that the introduction of Fe₃O₄ to GO decreased the surface area of the GO. However, MGO could be conveniently separated from the solution by magnetic field which increases its application prospects.

Adsorption kinetics

The adsorption kinetics reflect the state of the adsorption process throughout the whole adsorption reaction (Ho and McKay 1998). The mechanism of adsorption can be explored according to adsorption kinetic models. To reveal the most suitable mechanism for the adsorption process, pseudo-first- and pseudo-second-order models were used to analyze the adsorption data. The pseudo-first-order kinetic model is expressed as follows (Vadivelan and Kumar 2005):

$$\ln(q_e - q_t) = \ln q_e - k_1 t \quad (4)$$

The pseudo-second-order kinetic model is represented by the following (Ho 2006, Ho and McKay 1999, Vadivelan and Kumar 2005):

$$\frac{t}{q_t} = \frac{1}{k_2 q_e^2} + \frac{t}{q_t} \quad (5)$$

$$r = k_2 C \quad (6)$$

where q_e and q_t are the amounts of MB and CR adsorbed (mg g^{-1}) at equilibrium and at time t (min), respectively; k_1 is the pseudo-first-order rate constant (min^{-1}); k_2 is the pseudo-second-order rate constant ($\text{g mg}^{-1} \text{min}^{-1}$); C is the concentration of the solution (mg L^{-1}); and r is the rate of adsorption ($\text{g L}^{-1} \text{min}^{-1}$).

The correlation coefficients and rate constants of the pseudo-first- and pseudo-second-order model are shown in Table S2, and Fig. S4. It can be seen that the R^2 values of the pseudo-first-order model resulted in low correlation coefficients (0.5897 to 0.9835 for MB, 0.8988 to 0.9802 for CR). The R^2 values of the pseudo-second-order kinetic correlation coefficient were close to 0.9999, which is higher than the pseudo-first order kinetic correlation coefficient (Table S2, Fig. S4). There were great discrepancies between the theoretical adsorption capacities and the experimental data. The maximum theoretical adsorption capacities (505.05 mg g^{-1} for MB, 492.61 mg g^{-1} for CR) of the pseudo-second-order kinetics model were consistent with the experimentally measured data. Therefore, it can be concluded that the adsorption of MB and CR by MGO fitted the pseudo-second-order kinetic model well, and the adsorption process may be chemical adsorption.

Furthermore, as the initial concentration increased from 50 to 500 mg L^{-1} , the second-order rate constants (k_2) of adsorption for MB and CR were found to decrease from 3.95×10^{-2} to 1.0×10^{-3} ($\text{g mg}^{-1} \text{min}^{-1}$), and from 3.0×10^{-4} to 1.0×10^{-4} ($\text{g mg}^{-1} \text{min}^{-1}$), respectively. The reaction rate was related to the solution concentration, which was consistent with previously reported studies (Demirbas et al. 2009, Hanafiah et al. 2012).

Adsorption isotherms

The two adsorption models were used to interpret the adsorption isotherm at different concentrations and temperature ranges. The Langmuir and Freundlich sorption models were utilized to match the adsorption isotherms. The Langmuir isotherm model assumes that all adsorption sites are subjected to the same monolayer surface adsorption and that the adsorbed molecules are completely independent. The Freundlich model applies to multi-layer adsorption, and the adsorption capacity of varies from site to site.

The equation of the Langmuir isotherm is given as follows:

$$\frac{C_e}{q_e} = \frac{1}{k_L q_m} + \frac{C_e}{q_m} \quad (7)$$

where q_e is the amount of dye adsorbed (mg g^{-1}) at equilibrium, C_e is the equilibrium concentration of the solution (mg L^{-1}), q_m is the maximum adsorption capacity (mg g^{-1}), and k_L is the adsorption equilibrium constant (L mg^{-1}), which is related to the affinity of the binding site.

The Freundlich isotherm equation is expressed as follows:

$$\log q_e = \log k_F + \frac{1}{n} \log C_e \quad (8)$$

where k_F is the Freundlich constant, and n is the heterogeneity factor.

The theoretical correlation coefficient (R^2) parameters of the adsorption isotherms are presented in Table S3 and Fig. S5. The R^2 values of the Langmuir and Freundlich models are close to unity: 0.997 and 0.90 for MB and 0.995 and 0.94 for CR. These values imply that the Langmuir model may better describe the adsorption isotherm for the adsorption of these two different dyes. The correlation coefficient R^2 for the Langmuir equation is higher than the linear correlation coefficients for the Freundlich model. Furthermore, the theoretical maximum equilibrium adsorption capacity of the Langmuir equation for MB and CR was 613.50 and 909.09 mg g^{-1} at 328.15 K , respectively, which was closer to the experimental data. It was concluded that the adsorption of MB and CR by MGO was better described with the Langmuir model. The adsorption process was mainly monolayer uniform adsorption and mainly occurred on the functional groups of adsorption sites on the surface of MGO, such as hydroxyl, carboxyl, and epoxy functional groups. The monolayer coverage of dye molecules on the surface of the adsorbent may be explained at the molecular level. The structure of graphene oxide is layered, and there was no evidence of substitution taking place between different layers.

The maximum adsorption capacity of MGO increased from 546.45 mg g^{-1} (at 298.15 K) to 613.50 mg g^{-1} (at 328.15 K) for MB and from 628.93 mg g^{-1} (at 298.15 K) to

909.09 mg g⁻¹ (at 328.15 K) for CR, indicating that the adsorption capacity increased with increasing temperature (Table S4). This trend could be due to the enhanced mobility of the MB and CR molecules with rising temperature (Dawood 2012). The dye molecules may obtain adequate energy to interact with active sites at the surface of the adsorbent. The adsorption equilibrium constant k_L increased with increasing temperature and with greater adsorption capacity. This can be explained by the Brownian motion, which causes liquid molecules to move more intensely at higher temperature. Thus, the impact forces on dye particles by liquid molecules from different directions increase with rising temperature, resulting in increased adsorption capacity.

The suitability of the predicted adsorption model was informed by the value of the separation factor constant (R_L) which indicates the probability of the adsorption process. The separation factor (R_L) can be inferred from the Langmuir equation and indicates whether the adsorption process is favorable. The values of this parameter mean that the adsorption isotherm is unfavorable ($R_L > 1$), linear ($R_L = 1$), favorable ($0 < R_L < 1$), or irreversible ($R_L = 0$) (Chang et al. 2007, Vimonses et al. 2009). The separation factor (R_L) is defined as follows:

$$R_L = \frac{1}{1 + k_L C_0} \tag{9}$$

where k_L (L mg⁻¹) is the Langmuir constant, and C_0 (mg L⁻¹) is the initial dye concentration. In this study, the values of R_L were within the range of 0–1, indicating that the adsorption of MB, and CR onto MGO was a favorable process.

As an interesting material with enormous specific surface area, GO has abundant active sites that can effectively interact with dyes. The possible mechanism can be explained by electrostatic interact, hydrogen bonds, Van der Waals force and hydrophobic–hydrophobic interactions; a more in-depth explanation is as follows: (i) hydrogen bonds occur between the dye molecule and oxygen-containing hydroxyl (–OH) and carboxyl (–COOH) groups. (ii) Ion exchange occurs between the oxygen-containing groups (–OH, –COOH) in MGO and $D\text{-SO}_3^-$ ($D\text{-SO}_3^-$, D = dye molecule), forming $\text{MGO-COO-SO}_2\text{-D}$ and $\text{MGO-C-O-SO}_2\text{-D}$ (Guo et al. 2016). Guo et al. (2016) have reported that the -SO_3^- groups of CR are involved in the adsorption process. (iii) The protonation of –COOH and –OH occurred on the surface of MGO in acidic solution (i.e., $\text{MGO-OH} + \text{H}^+ \leftrightarrow \text{MGO-OH}_2^+$) (Ahmad and Kumar 2010).

Thermodynamic study

To evaluate the effect of temperature on adsorption process, the thermodynamic parameters Gibbs free energy (ΔG^0 ,

Table 1 Thermodynamic parameters for MB and CR adsorption onto MGO

Dye	Temperature (K)	ΔG^0 (kJ mol ⁻¹)	ΔH^0 (kJ mol ⁻¹)	ΔS^0 (J K ⁻¹ mol ⁻¹)
MB	298.15	–28.23	113.14	474.16
	308.15	–32.97		
	318.15	–37.71		
	328.15	–42.46		
CR	298.15	–21.87	41.83	213.65
	308.15	–24.00		
	318.15	–26.14		
	328.15	–28.28		

enthalpy (ΔH^0 , kJ mol⁻¹), and entropy (ΔS^0 , kJ mol⁻¹ K⁻¹) can be calculated by the following equations:

$$\ln(k_L) = \frac{\Delta S^0}{R} - \frac{\Delta H^0}{RT} \tag{10}$$

$$k_L = \frac{q_e}{c_e} \tag{11}$$

$$\Delta G^0 = \Delta H^0 - T\Delta S^0 \tag{12}$$

where k_L is the Langmuir constant (L g⁻¹), R is the universal gas constant (8.314 J mol⁻¹ K⁻¹), and T is the absolute temperature (K).

Table 1 shows the thermodynamic parameters of the adsorption. The negative values of ΔG^0 indicated that the adsorption reaction can be carried out at room temperature and the decrease of ΔG^0 with increasing temperature indicated that the adsorption reaction was spontaneous at higher temperatures. The values of ΔH^0 and ΔS^0 were found to be 113.14 and 474.16 J K⁻¹ mol⁻¹ for MB and 41.83 and 213.65 J K⁻¹ mol⁻¹

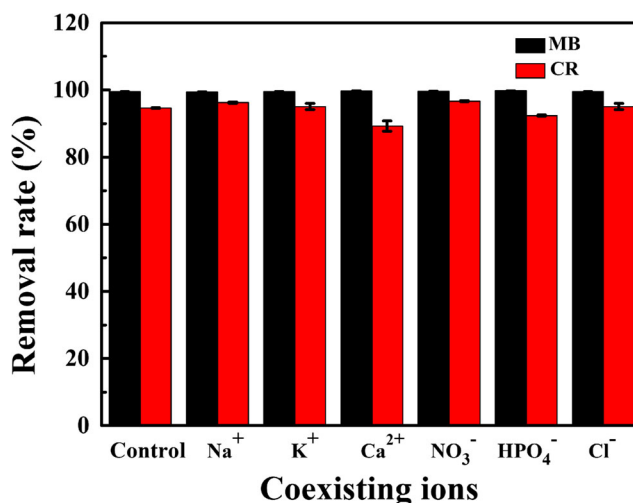


Fig. 5 Effect of coexisting ions. Conditions: adsorbent dosage 0.5 g L⁻¹; temperature 298 ± 0.5 K; stirring rate 180 rpm; initial dye concentrations 100 mg L⁻¹; Na⁺, Ca²⁺, K⁺, and NO₃⁻, Cl⁻, and HPO₄⁻ concentrations 1 mol L⁻¹

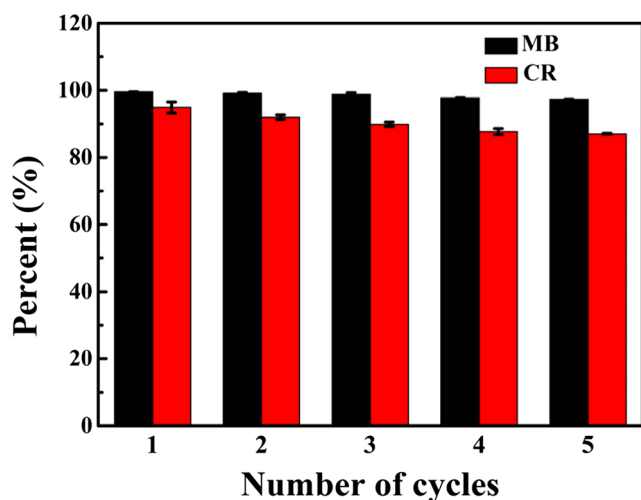


Fig. 6 Regeneration and reuse of MGO. Conditions: adsorbent dosage 0.5 g L^{-1} ; temperature $298 \pm 0.5 \text{ K}$; stirring rate 180 rpm ; initial concentrations 50 mg L^{-1}

for CR, respectively. The positive values of ΔH^0 and ΔS^0 showed that the adsorption of MB and CR by MGO is endothermic. Therefore, the prepared MGO could be effectively used in dye adsorption without harsh reaction conditions, indicating that the adsorbent has the potential possibility to be used in practical wastewater treatment.

Effect of coexisting ions

In practical applications, the large amount of dissolved metal cations and inorganic anions, such as Na^+ , Ca^{2+} , K^+ , NO_3^- , Cl^- , and HPO_4^- , may greatly affect the adsorption process. Therefore, the effect of individual coexisting ions (1 mol L^{-1}) on the adsorption of MB and CR was investigated in series. Figure 5 summarizes the effect of the common coexisting metal cations Na^+ , Ca^{2+} , and K^+ and inorganic anions NO_3^- , Cl^- , and HPO_4^- , all of which showed no significant effects on MB/CR adsorption. Hence, MGO composites could serve as an effective adsorbent for dye wastewater remediation.

Table 2 Comparison of MGO with other graphene-based adsorbents

Adsorbents	Adsorbate	Qm (mg g^{-1})	References
Cellulose/graphene oxide	MB	480.77	(Chen et al. 2016)
Hydroxo aluminum/graphene	CR	497.51	(Wu et al. 2014)
Graphene oxide/chitosan fibers	CR	294.12	(Du et al. 2014)
Beta-cyclodextrin and GO gel (SCGG)	MB	133.24	(Wu et al. 2017)
$\text{Fe}_3\text{O}_4@/\text{SiO}_2@/\text{CS-TETA-GO}$	MB	529.1	(Wang et al. 2017)
Magnetic GO/poly(vinyl alcohol) (PVA) composite gels	MB	231.12	(Cheng et al. 2015)
Magnetic rGO-loaded hydrogels	MB	111.9	(Halouane et al. 2017)
Magnetic graphene oxide	MB/CR	546.45/ 628.93	This study

Desorption and regeneration

The continuous recycle experiments were conducted to evaluate the stability and the application potential of the prepared adsorbent. The obtained MGO particles were added to the MB/CR solution (50 mg L^{-1}), and the residual concentration was measured after reaching adsorption equilibrium. Distilled water and NaOH were used to desorb dye several times until no more leaching dye could be detected. The adsorption rates of MB and CR still were maintained at 97.43% and 87.23% after five successive adsorption-desorption cycles (Fig. 6). These results indicated that the performance of MGO was not appreciably impaired after five cycles, which illustrated its good stability and practical application potential.

Table 2 compares the maximum adsorption capacity of graphene-based adsorbents for dye removal under different experimental conditions. The maximum adsorption capacities of dyes on MGO in this study were better than those of most previously studied graphene-based materials. MGO has a slight advantage in adsorption capacity. Since it could also be efficiently recycled and reused, MGO has broad practical application prospects in the treatment of organic pollutants.

Conclusions

In summary, a feasible, economical and green route for the removal of two typical dyes by a magnetic graphene oxide/ Fe_3O_4 (MGO) nanocomposite was demonstrated. The results showed that the MGO exhibited a great adsorption ability for dye removal and could adapt to a wide pH range from 5 to 11. The adsorption behavior was best suited for the Langmuir adsorption isotherm equation, showing calculated maximum adsorption capacity of 546.45 and 628.93 mg g^{-1} for MB and CR, respectively. The adsorption process fit the pseudo-second-order kinetic model well, which revealed that it might be the chemical interaction between adsorbate and adsorbent. Furthermore, the prepared MGO nanoparticles maintained good stability after five successive adsorption-desorption cycles. The results show

that this “green” magnetic graphene oxide adsorbent has a good stability and high adsorption capacity and may serve as a promising adsorbent for wastewater purification.

Acknowledgments The authors thank Prof. Anatoly Zinchenko for a helpful discussion.

Funding This work was supported by the National Natural Science Foundation of China (Nos. 41772264, 51408074) and the Research Fund of State Key Laboratory of Geohazard Prevention and Geoenvironment Protection (SKLGP2017Z009).

Compliance with ethical standards

Conflict of interest The authors declare that there is no conflict of interests regarding the publication of this paper.

References

- Abidi N, Errais E, Duplay J, Berez A, Jrad A, Schaefer G, Ghazi M, Semhi K, Trabelsi-Ayadi M (2015) Treatment of dye-containing effluent by natural clay. *J Clean Prod* 86:432–440
- Ahmad R, Kumar R (2010) Adsorptive removal of Congo red dye from aqueous solution using bael shell carbon. *Appl Surf Sci* 257:1628–1633
- Akbari A, Remigy JC, Aptel P (2002) Treatment of textile dye effluent using a polyamide-based nanofiltration membrane. *Chem Eng Process* 41:601–609
- Aliyari E, Alvand M, Shemirani F (2016) Modified surface-active ionic liquid-coated magnetic graphene oxide as a new magnetic solid phase extraction sorbent for preconcentration of trace nickel. *RSC Adv* 6:64193–64202
- Barathi M, Kumar ASK, Kumar CU, Rajesh N (2014) Graphene oxide-aluminium oxyhydroxide interaction and its application for the effective adsorption of fluoride. *RSC Adv* 4:53711–53721
- Belpaire C, Reyns T, Geeraerts C, Van Loco J (2015) Toxic textile dyes accumulate in wild European eel *Anguilla anguilla*. *Chemosphere* 138:784–791
- Chang Y-H, Huang C-F, Hsu W-J, Chang F-C (2007) Removal of Hg²⁺ from aqueous solution using alginate gel containing chitosan. *J Appl Polym Sci* 104:2896–2905
- Chen L, Li YH, Hu S, Sun JK, Du QJ, Yang XX, Ji Q, Wang ZH, Wang DC, Xia YZ (2016) Removal of methylene blue from water by cellulose/graphene oxide fibres. *J Exp Nanosci* 11:1156–1170
- Cheng Z, Liao J, He B, Zhang F, Zhang F, Huang X, Zhou L (2015) One-step fabrication of graphene oxide enhanced magnetic composite gel for highly efficient dye adsorption and catalysis. *ACS Sustain Chem Eng* 3:1677–1685
- Cheng ZL, Li W, Wu PR, Liu Z (2017) A strategy for preparing modified graphene oxide with good dispersibility and transparency in oil. *Ind Eng Chem Res* 56:5527–5534
- Dawood SS, Sen TK (2012) Removal of anionic dye Congo red from aqueous solution by raw pine and acid-treated pine cone powder as adsorbent: equilibrium, thermodynamic, kinetics, mechanism and process design. *Water Res* 46:1933–1946
- Demirbas E, Dizge N, Sulak MT, Kobya M (2009) Adsorption kinetics and equilibrium of copper from aqueous solutions using hazelnut shell activated carbon. *Chem Eng J* 148:480–487
- Dizaji AK, Mortaheb HR, Mokhtarani B (2016) Noncovalently functionalized graphene oxide/graphene with imidazolium-based ionic liquids for adsorptive removal of dibenzothiophene from model fuel. *J Mater Sci* 51:10092–10103
- Dreyer DR, Park S, Bielawski CW, Ruoff RS (2010) The chemistry of graphene oxide. *Chem Soc Rev* 39:228–240
- Du Q, Sun J, Li Y, Yang X, Wang X, Wang Z, Xia L (2014) Highly enhanced adsorption of Congo red onto graphene oxide/chitosan fibers by wet-chemical etching off silica nanoparticles. *Chem Eng J* 245:99–106
- Forgacs E, Cserhati T, Oros G (2004) Removal of synthetic dyes from wastewaters: a review. *Environ Int* 30:953–971
- Greenwald MJ, Redding AM, Cannon FS (2015) A rapid kinetic dye test to predict the adsorption of 2-methylisoborneol onto granular activated carbons and to identify the influence of pore volume distributions. *Water Res* 68:784–792
- Guo YF, Deng J, Zhu JY, Zhou C, Zhou CY, Zhou XJ, Bai RB (2016) Removal of anionic azo dye from water with activated graphene oxide: kinetic, equilibrium and thermodynamic modeling. *RSC Adv* 6:39762–39773
- Halouane F, Oz Y, Mezziane D, Barras A, Juraszek J, Singh SK, Kurungot S, Shaw PK, Sanyal R, Boukherroub R, Sanyal A, Szunerits S (2017) Magnetic reduced graphene oxide loaded hydrogels: highly versatile and efficient adsorbents for dyes and selective Cr(VI) ions removal. *J Colloid Interf Sci* 507:360–369
- Hanafiah M, Ngah WSW, Zolkafly SH, Teong LC, Majid ZAA (2012) Acid blue 25 adsorption on base treated *Shorea dasyphylla* sawdust: kinetic, isotherm, thermodynamic and spectroscopic analysis. *J Environ Sci* 24:261–268
- Ho YS (2006) Second-order kinetic model for the sorption of cadmium onto tree fern: a comparison of linear and non-linear methods. *Water Res* 40:119–125
- Ho YS, McKay G (1998) Kinetic models for the sorption of dye from aqueous solution by wood. *Process Saf Environ* 76:183–191
- Ho YS, McKay G (1999) Pseudo-second order model for sorption processes. *Process Biochem* 34:451–465
- Huang GJ, Chen ZG, Li MD, Yang B, Xin ML, Li SP, Yin ZJ (2016) Surface functional modification of graphene and graphene oxide. *Acta Chim Sin* 74:789–799
- Kyzas GZ, Fu J, Matis KA (2013) The change from past to future for adsorbent materials in treatment of dyeing wastewaters. *Materials* 6: 5131–5158
- Liu T, Li Y, Du Q, Sun J, Jiao Y, Yang G, Wang Z, Xia Y, Zhang W, Wang K, Zhu H, Wu D (2012) Adsorption of methylene blue from aqueous solution by graphene. *Colloids Surf B Biointerfaces* 90:197–203
- Lucas MS, Peres JA (2006) Decolorization of the azo dye reactive black 5 by Fenton and photo-Fenton oxidation. *Dyes Pigments* 71:236–244
- Ma X, Chen PL, Zhou M, Zhong ZX, Zhang F, Xing WH (2017) Tight ultrafiltration ceramic membrane for separation of dyes and mixed salts (both NaCl/Na₂SO₄) in textile wastewater treatment. *Ind Eng Chem Res* 56:7070–7079
- Ma H, Pu S, Ma J, Yan C, Zinchenko A, Pei X, Chu W (2018) Formation of multi-layered chitosan honeycomb spheres via breath-figure-like approach in combination with co-precipitation processing. *Mater Lett* 211:91–95
- Malachova K, Rybkova Z, Sezimova H, Cerven J, Novotny C (2013) Biodegradation and detoxification potential of rotating biological contactor (RBC) with *Irpex lacteus* for remediation of dye-containing wastewater. *Water Res* 47:7143–7148
- Netpradit S, Thiravetyan P, Towprayoon S (2003) Application of ‘waste’ metal hydroxide sludge for adsorption of azo reactive dyes. *Water Res* 37:763–772
- Peng R, Chen X, Ghosh R (2017a) Preparation of graphene oxide-cotton fiber composite adsorbent and its application for the purification of polyphenols from pomegranate peel extract. *Sep Purif Technol* 174: 561–569
- Peng W, Li H, Liu Y, Song S (2017b) A review on heavy metal ions adsorption from water by graphene oxide and its composites. *J Mol Liq* 230:496–504

- Pu S, Xiang C, Zhu R, Ma H, Zinchenko A, Chu W (2017a) An efficient heterogeneous Fenton catalyst based on modified diatomite for degradation of cationic dye simulated wastewater. *Desalin Water Treat* 79:378–385
- Pu S, Zhu R, Ma H, Deng D, Pei X, Qi F, Chu W (2017b) Facile in-situ design strategy to disperse TiO₂ nanoparticles on graphene for the enhanced photocatalytic degradation of rhodamine 6G. *Applied Catalysis B-Environmental* 218:208–219
- Pu SY, Ma H, Zinchenko A, Chu W (2017d) Novel highly porous magnetic hydrogel beads composed of chitosan and sodium citrate: an effective adsorbent for the removal of heavy metals from aqueous solutions. *Environ Sci Pollut R* 24:16520–16530
- Ren Y, Abbood HA, He F, Peng H, Huang K (2013) Magnetic EDTA-modified chitosan/SiO₂/Fe₃O₄ adsorbent: preparation, characterization, and application in heavy metal adsorption. *Chem Eng J* 226:300–311
- Riera-Torres M, Gutierrez-Bouzan MC, Morell JV, Lis MJ, Crespi M (2011) Influence of electrochemical pre-treatment in dyeing wastewater reuse for five reactive dyes. *Text Res J* 81:1926–1939
- Stankovich S, Dikin DA, Dommett GHB, Kohlhaas KM, Zimney EJ, Stach EA, Piner RD, Nguyen ST, Ruoff RS (2006) Graphene-based composite materials. *Nature* 442:282–286
- Szpyrkowicz L, Juzzolino C, Kaul SN (2001) A comparative study on oxidation of disperse dyes by electrochemical process, ozone, hypochlorite and Fenton reagent. *Water Res* 35:2129–2136
- Tang ZH, Shen SL, Zhuang J, Wang X (2010) Noble-metal-promoted three-dimensional macroassembly of single-layered graphene oxide. *Angew Chem Int Edit* 49:4603–4607
- Vadivelan V, Kumar KV (2005) Equilibrium, kinetics, mechanism, and process design for the sorption of methylene blue onto rice husk. *J Colloid Interf Sci* 286:90–100
- Vimonses V, Lei S, Jin B, Chow CWK, Saint C (2009) Kinetic study and equilibrium isotherm analysis of Congo red adsorption by clay materials. *Chem Eng J* 148:354–364
- Wan Z, Wang JL (2017) Degradation of sulfamethazine using Fe₃O₄-Mn₃O₄/reduced graphene oxide hybrid as Fenton-like catalyst. *J Hazard Mater* 324:653–664
- Wang H, Yuan XZ, Wu Y, Chen XH, Leng LJ, Wang H, Li H, Zeng GM (2015) Facile synthesis of polypyrrole decorated reduced graphene oxide-Fe₃O₄ magnetic composites and its application for the Cr(VI) removal. *Chem Eng J* 262:597–606
- Wang F, Zhang LJ, Wang YY, Liu XJ, Rohani S, Lu J (2017) Fe₃O₄@SiO₂@CS-TETA functionalized graphene oxide for the adsorption of methylene blue (MB) and Cu(II). *Appl Surf Sci* 420: 970–981
- Wu Y, Luo HJ, Wang H (2014) Efficient removal of Congo red from aqueous solutions by surfactant-modified Hydroxyl aluminum/graphene composites. *Sep Sci Technol* 49:2700–2710
- Wu YC, Qi HJ, Shi C, Ma RX, Liu SX, Huang ZH (2017) Preparation and adsorption behaviors of sodium alginate-based adsorbent-immobilized beta-cyclodextrin and graphene oxide. *RSC Adv* 7: 31549–31557
- Yang CH, Wang CY, Huang KS, Yeh CS, Wang AHJ, Wang WT, Lin MY (2012): Facile synthesis of radial-like macroporous superparamagnetic chitosan spheres with in-situ co-precipitation and gelation of Ferro-gels. *PLoS One* 7, 7
- Yao YJ, Miao SD, Liu SZ, Ma LP, Sun HQ, Wang SB (2012) Synthesis, characterization, and adsorption properties of magnetic Fe₃O₄@graphene nanocomposite. *Chem Eng J* 184:326–332
- Zhang WJ, Zhou CJ, Zhou WC, Lei AH, Zhang QL, Wan Q, Zou BS (2011) Fast and considerable adsorption of methylene blue dye onto graphene oxide. *Bull Environ Contam Toxicol* 87:86–90
- Zhang LY, Zhang W, Zhou Z, Li CM (2016) Gamma-Fe₂O₃ nanocrystals-anchored macro/meso-porous graphene as a highly efficient adsorbent toward removal of methylene blue. *J Colloid Interface Sci* 476:200–205